Biochimica et Biophysica Acta 1840 (2014) 357–366

Contents lists available at ScienceDirect

Biochimica et Biophysica Acta

journal homepage: www.elsevier.com/locate/bbagen

Stabilities and structures of islet amyloid polypeptide ($IAPP_{22-28}$) oligomers: From dimer to 16-mer

Jingjing Guo [a,b,c], Yan Zhang [a], Lulu Ning [b,c], Pingzu Jiao [a], Huanxiang Liu [a,b,c,*], Xiaojun Yao [b,c,*]

[a] School of Pharmacy, Lanzhou University, Lanzhou 730000, China
[b] State Key Laboratory of Applied Organic Chemistry, Lanzhou University, Lanzhou 730000, China
[c] Department of Chemistry, Lanzhou University, Lanzhou 730000, China

ARTICLE INFO

Article history:
Received 6 February 2013
Received in revised form 11 August 2013
Accepted 6 September 2013
Available online 14 September 2013

Keywords:
Nucleation
Amyloid fibril
Molecular dynamics simulation
Islet amyloid polypeptide (residues 22-28)
Type II diabetes

ABSTRACT

Background: The formation of amyloid fibrils is associated with many age-related degenerative diseases. Nevertheless, the molecular mechanism that directs the nucleation of these fibrils is not fully understood.
Methods: Here, we performed MD simulations for the NFGAILS motif of hIAPP associated with the type II diabetes to estimate the stabilities of $hIAPP_{22-28}$ protofibrils with different sizes: from 2 to 16 chains. In addition, to study the initial self-assembly stage, 4 and 8 $IAPP_{22-28}$ chains in explicit solvent were also simulated.
Results: Our results indicate that the ordered protofibrils with no more than 16 $hIAPP_{22-28}$ chains will be structurally stable in two layers, while one-layer or three-layer models are not stable as expected. Furthermore, the oligomerization simulations show that the initial coil structures of peptides can quickly aggregate and convert to partially ordered β-sheet-rich oligomers.
Conclusions: Based on the obtained results, we found that the stability of an $IAPP_{22-28}$ oligomer was not only related with its size but also with its morphology. The driving forces to form and stabilize an oligomer are the hydrophobic effects and backbone H-bond interaction. Our simulations also indicate that $IAPP_{22-28}$ peptides tend to form an antiparallel strand orientation within the sheet.
General significance: Our finding can not only enhance the understanding about potential mechanisms of hIAPP nuclei formation and the extensive structural polymorphisms of oligomers, but also provide valuable information to develop potential β-sheet formation inhibitors against type II diabetes.

1. Introduction

Amyloidogenesis is a common pathogenic process associated with many age-related degenerative diseases, including Alzheimer's disease, Parkinson's disease, Huntington's diseases, and type II diabetes [1–4], which share a striking number of common pathological features or events, such as evidence of membrane damage, oxidative stress, mitochondrial dysfunction, upregulation of autophagy and cell death. In these diseases, proteins or peptides of diverse sequences form toxic soluble oligomers and insoluble amyloid fibrils, sharing a highly similar "cross-β" spine and suggesting a common mechanism [4,5]. The atomic architecture of a spine has been revealed, showing that it is a pair of β-sheets, with the facing side chains of the two sheets interdigitated into a dry 'steric zipper'. Sawaya et al. [6] summarized more than 30 segments from fibril-forming proteins which can form amyloid-like fibrils, microcrystals, or usually both, and also suggested that common structural features were shared by amyloid diseases at the molecular level.

Studies have further suggested that amyloid fibril formation has many characteristics of a "nucleated growth" mechanism [1]. Once a nucleus is formed, fibril growth is thought to proceed rapidly by further association of either monomers or oligomers. However, the structural characteristics and oligomer size of this ensemble of fibril nucleating species have yet to be determined, and the mechanism of further fibril elongation is unclear. This is due, in part, to the limited access of experimental characterization to this earliest aggregation stage, thus providing an opportunity for theoretical studies to bridge the experimental gap between the monomer, oligomer and fibril. Now many computational studies have focused on the fibril-formation mechanism. For example, atomistic models have been employed to study the conformational space of amyloidogenic polypeptides in the monomeric state or dimer [7–9], the nucleation phase or fibril formation [10–18], the structural stability of fibril model [19–21], and the elongation phase [22–24].

It is well known that atomistic molecular dynamics simulation is a versatile tool for studying protein misfolding and aggregation. However, one of its major challenges is choosing an appropriate force field as different force fields have possible biases toward certain types of secondary structure [25–32]. Some recent studies have indicated that

Abbreviations: hIAPP, human islet amyloid polypeptide; MD, molecular dynamics

* Corresponding authors at: State Key Laboratory of Applied Organic Chemistry, Lanzhou University, Lanzhou 730000, China. Tel.: +86 931 891 2578; fax: +86 931 891 2582.
E-mail addresses: hxliu@lzu.edu.cn (H. Liu), xjyao@lzu.edu.cn (X. Yao).

0304-4165/$ – see front matter © 2013 Elsevier B.V. All rights reserved.
http://dx.doi.org/10.1016/j.bbagen.2013.09.012

modern MD force fields slightly overestimate the presence of helical structure in small peptides [25,32]. Nevertheless, an uncapped peptide can fold into a native-like β-hairpin structure at 310 K when Amber ff03 or other seven force fields were used, such as Amber ff99SB-ILDN, Amber ff99SB*-ILDN, Amber ff99SB, Amber ff99SB*, Amber ff03, Amber ff03*, GROMOS96 43a1p, and GROMOS96 53a6 [26]. Furthermore, the simulations based on CHARMM27 force field were able to form native hairpins in some of the elevated temperature simulations, while the OPLS-AA/L ones did not yield native hairpin structures at any temperatures tested [26].

Islet amyloid polypeptide (IAPP, or amylin) is a hormone coexpressed with insulin by pancreatic islet β-cells and its abnormal aggregation into amyloid fibrils is a hallmark of type II diabetes [33]. Conversion from soluble monomer, IAPP(1–37), to β-sheet fibrils involves changes in the molecular conformation, cellular biochemistry and diabetes-related factors [34]. For reasons not clearly understood, human IAPP (hIAPP) aggregates in type II diabetes to form oligomers that have cytotoxic properties and interfere with beta-cell function, eventually leading to the loss of insulin production [35].

As the appearance of IAPP fibrils in pancreatic tissue is a hallmark of diabetes type II, to design therapeutic agents to combat the progression of diabetes type II, it is worthwhile to investigate the mechanisms of the IAPP fibril growth. The central region of amylin, residues 20–29 (SNNFGAILSS), has been implicated as a key determinant of amyloid formation. Previous experimental results indicate that residues 22, 24, and 26–28 play a key role in formation of amyloid by amylin [36]. Positions 23 and 25 also appear to be important, but may be less critical than positions 22, 24, and 26–28 [36]. These results may help to understand the formation of hIAPP amyloid, however, the mechanisms of how the seed forms and the extensive structural polymorphism of oligomers are still not fully understood. These questions have unique, indispensable values for understanding the pathogenesis and designing the inhibitors against type 2 diabetes. Due to the importance of nuclei in the formation of amyloid, in this work, we present a systematic study with standard molecular dynamics simulation aimed at investigating the characteristics of the nuclei and structural stabilities of $hIAPP_{22-28}$ oligomers.

2. Methods

For steric zippers of $hIAPP_{20-29}$ peptide, the spine can be either parallel or antiparallel within each β-sheet strand and also parallel or antiparallel between each sheet [37,38], and their differences might depend on different sample preparations or initial seedings. Here, we built our model systems in a similar way with Yang and Zhou [39]. The intersheet space was set to 10.5 Å, and the interstand space was set to 4.87 Å. However, in our current study, we mainly considered the stabilities of the $hIAPP_{22-28}$ steric zipper which shares a basic unit of two parallel, in-register β-sheets with their different sides facing each other ('face-to-back' or 'up to down') and each sheet composed of antiparallel β-strands based on the full high-resolution structure of antiparallel $IAPP_{22-28}$ fibrils (PDB ID: 2KIB) [38]. The model is an antiparallel ladder "hetero zipper"; the peptides in one β-sheet are antiparallel, and the sheets are parallel so that the two faces of the protofibril are different (Fig. 1). Here, we estimate the stabilities of different size protofibrils formed by $IAPP_{22-28}$ peptide: from 2 chains to 16 chains (Table 1). In addition, to study the initial self-assembly stage, 4 and 8 $IAPP_{22-28}$ chains in explicit solvent were also simulated. In our simulations, the N- and C-termini of $IAPP_{22-28}$ are capped, respectively, by neutral acetyl and methylamino groups.

The different oligomer models were first placed in a cubic box with periodic boundary conditions, and the distance between the model and the box edges was set to be about 1.0 nm. Initial configurations were minimized in three steps, first keeping the peptides fixed, and then only keeping the backbones fixed, and finally keeping all of the molecules free.

All MD simulations were carried out using the AMBER 10.0 package [40] together with the ff03 force field [41,42]. The TIP3P [43] solvent model was used to describe water molecule. A 2 fs time step was used to integrate the equations of motion with the Verlet leapfrog algorithm. The long-range electrostatic interactions were treated with the particle mesh Ewald method [44]. A nonbonded pair list cutoff of 1.0 nm was used. The SHAKE algorithm [45] was used to constrain all bond lengths. Temperature (310 K) and pressure (1 atm) were controlled by the Berendsen thermostat and barostat [46] with coupling constants of 0.1 and 1.0 ps, respectively. For all simulations, the atomic coordinates were saved every 2 ps for analysis.

The trajectories were analyzed using amber [40] and VMD [47] programs. The STRIDE algorithm [48] was used to assign secondary structures. To evaluate the hydrogen-bond (H-bond) preference of each residue of $IAPP_{22-28}$, backbone H-bonds were considered by using VMD [47]. One backbone H-bond is taken as formed if the N…O distance is less than 0.35 nm and the N–H…O angle is greater than 150° [49].

3. Results

3.1. Structural stabilities of $hIAPP_{22-28}$ oligomers with different size

3.1.1. Overall structural stabilities

We performed all-atom molecular dynamics simulations with a number of $IAPP_{22-28}$ fragments ranging from 2 to 16, arranged in a single, double, or triple layer (see Table 1). The peptides were capped with ACE and NME at two ends, respectively. All simulations were performed for 50 ns. In Table 1, the initial and final configurations of all systems are presented. As can be seen, final single layer models of 2 and 4 chains lost their native β-sheet structures completely, which suggests single layer β-sheets were unstable. Although double layer model of 6 chains mainly maintained its high β-sheet contents after 50 ns simulations, its structure was completely dislocated. For other double layer models, as a whole, they were relatively stable, although one of the edge chains

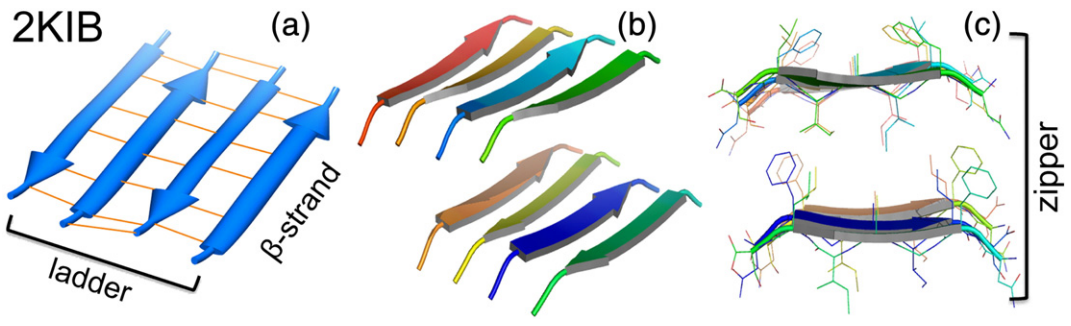

Fig. 1. Cartoon representation of the respective NMR $IAPP_{22-28}$ fibril (PDB ID: 2KIB). a) β-Strands are arranged by hydrogen bonding (shown as orange lines) into a ladder, which is antiparallel here. b, c) Two ladders combine into a steric zipper. Atoms are shown as lines without hydrogen atom in Fig. 1c.

Table 1
Structural evolution during the MD simulation of several configurations of $IAPP_{22-28}$ system with different number of chains (ranging between 2 and 16). The second column reports the number of chains. The third column is a schematic representation of the starting configuration, in which the gray layers are β-sheets, the circle with a central dot represents a β-strand pointing outside the paper plane, and the circle with a cross represents a β-strand pointing inside the paper plane. The third and fourth columns are cartoon representation of the structures before and after the MD simulation. The fifth one shows the number of trajectories. The last column is the simulation time.

Layer	System	Starting configuration	Final configuration	Trajectories	Simulation time
Single layer	2 chains Dimer			1	50 ns
	4 chains Tetramer			1	50 ns
Double layer	6 chains Hexamer			1	50 ns
	8 chains Octamer			3	50 ns
	10 chains Decamer			3	50 ns
	12 chains 12-mer1			3	50 ns
	14 chains 14-mer			3	50 ns
	16 chains 16-mer			3	50 ns
Triple layer	9 chains Nonamer			2	50 ns
	12 chains 12-mer2		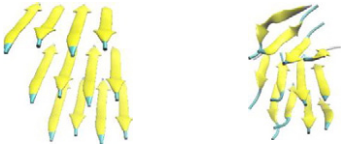	2	50 ns
	15 chains 15-mer			2	50 ns

was lost in some runs. We also performed simulations for triple layer models with 9, 12 and 15 $IAPP_{22-28}$ chains. The initial and final structures of them can be seen in Fig. S1. Most of the peptides in three-layer models maintained their β-sheet conformations, but the sheets twisted around the axis perpendicular to the β-sheets. Hence, the stability of an $IAPP_{22-28}$ oligomer is not only related with its size but also with its morphology.

Cα root-mean-square fluctuations (RMSFs) around the first structure for the last 25 ns were calculated and averaged for each chain in all runs since they can give an indication of backbone flexibility and mobility of $IAPP_{22-28}$. The results of averaged RMSFs for different systems are shown in Fig. 2. As can be seen, the single layer with 4 chains has the largest RMSF values, while RMSF values of the dimer are relatively small during the last 25 ns. For all systems of double layer and triple layer, Cα RMSFs fluctuate in a very similar manner and the RMSF values are almost smaller than 2 Å, especially the middle residues of $IAPP_{22-28}$ fragment. Therefore, we can conclude that during the last 25 ns the double layer and triple layer models are relatively stable, and the single layer with 4 chains having the largest backbone flexibility and mobility is the most instable one.

The equilibration of the MD trajectories for the systems with more than 8 chains was further tested based on the convergence of the averaged backbone H-bond numbers and the contact numbers between sheets. As can be seen in Fig. S2, their relative fluctuations were very small during the last 25 ns, especially the last 15 ns, hence the studied systems were up to convergence in 50 ns. To further test whether our simulations converged over the 50-ns time scale, we elongated some trajectories to 100 ns, such as two-layer models with 8 and 10 chains

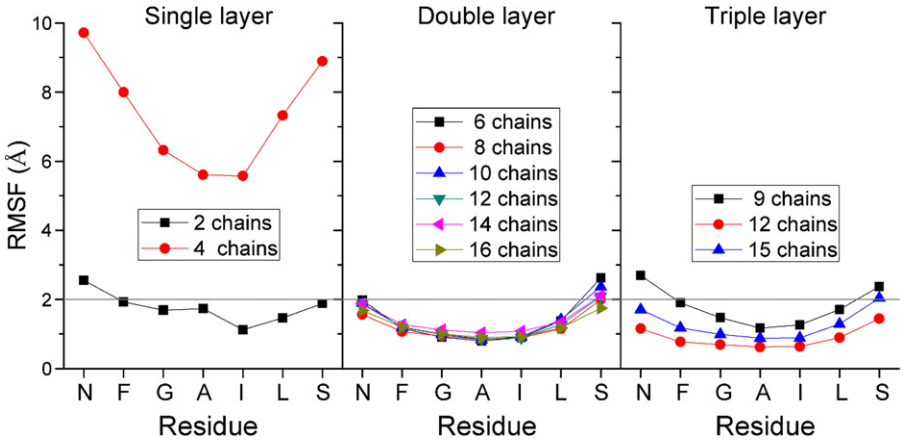

Fig. 2. Averaged Cα root-mean-square fluctuations (RMSFs) around the first structure for the last 25 ns for each chain in all runs.

and three-layer models with 12 and 15 chains. By comparing the snapshots at 100 ns extracted from the elongated trajectories with the corresponding snapshots at 50 ns, we find that almost nothing has changed in these oligomers (Fig. S3), indicating that in our present work, our simulations are converged in 50 ns.

3.1.2. Backbone hydrogen-bond map and contact map between sheets

As we know, amyloid fibrils are generally formed by peptides in extended conformations (β-strands) into β-sheets through parallel or antiparallel backbone hydrogen bonding bridges, which further stack tightly through steric effects at a completely dry interface, called a zipper [6]. Here, the β-strands of $IAPP_{22–28}$ are arranged by backbone hydrogen bonds into a ladder, which is antiparallel, and then the ladders combine into a steric zipper (Fig. 1a). Therefore the details of changes in ladders or sheets can be seen from backbone H-bond information, while the contacts between side chains in different sheets can be used to investigate the interaction between sheets. Here, two amino acids are considered to form a contact if the distance between their side-chain atoms is within 3.2 Å.

Fig. 3 shows the main-chain H-bond contact map where the strength of contacts is proportional to the number of H-bonds between two amino acids. In each system, the largest H-bond number is considered as 1 for reference. As the β-strands are antiparallel in a ladder, one residue in $IAPP_{22–28}$ should form H-bond with another one on the contrary. In most trajectories, H-bond between G24 and I26 is strongest, and the one between F23 and L27 is also very strong, which suggest that these four residues may play a key role to help stabilize the already existing β-sheets. A disordered H-bond map means that the ladders are unstable. As can be seen, most of the double and triple models have very similar H-bond maps, indicating that these models can be stable in solution, while single layer models with disordered H-bond maps are unstable. Furthermore, the H-bond maps also show that 6, 8, and 9 chain models have some additional hydrogen bonds, implying their weaker stabilities than those of the other double and triple models.

Just as Fig. 1c shows, in a double layer model, the interfaces of two sheets are different. In Fig. 4, for one sheet, N22, G24, I26 and S28 are buried in the interface, while for the other one, F23, A25 and L27 are buried. However, as the side chain of G24 only has one hydrogen atom, G24 almost has no contact with the other sheet. As for the terminal residues, N22 and S28, they are more flexible, so their interactions in the stacking are much smaller than those of I26. Therefore, in sheet A, I26 is the most important residue. In sheet B, as can be seen in Fig. 5, F23, A25 and L27 all have obvious interaction with I26, especially F23. Residues F23, A25, I26 and L27 are all hydrophobic, and they are major components of the interface inside the seeds. Hence, we can infer that hydrophobic interaction plays an important role in the seed formation of $IAPP_{22–28}$. Furthermore, for the model with 6 chains, its contact map is disordered compared with the other models, indicating that it is the most unstable model. We can see from Fig. 5 that for triple layer models, the middle sheet has two different interfaces with sheet A and sheet C, and the two contact maps in the same model are very complementary. More specifically, hydrophobic residues F23, A25, I26 and L27 are vital in the stacking interaction, the same as in the double layer models.

As Fig. 3 shows, the three-layer model with 12 peptides has weaker inter-strand H-bond interaction than the two-layer model with 8 peptides in the middle of the peptide, which can also be found in models with 5 chains per sheet. As for the inter-sheet interaction, ideally an oligomer should have a contact map like that of the two-layer model with 16 chains. By comparing the two-layer and three-layer models with 4 or 5 chains in one sheet, we find that the contact map of two layer models is more ordered and closer to the ideal one (Figs. 4 and 5).

3.1.3. Changes of secondary structures

Furthermore, we investigated the secondary structural stability of the studied oligomers with different sizes, and the β-sheet contents are plotted as a function of simulation time in Fig. S4. The analysis of secondary structures is very useful for further understanding of the stability of β-sheets. Our results show that the β-sheet contents for single layer models fluctuate wildly indicating that they are unstable. However, it can be seen that the double and triple layer models adapt quite well to the native β-sheet-rich structure with β-sheet contents about 60%.

In order to investigate the β-sheet content of each residue, we averaged the secondary structure information to each residue for each run in the last 10 ns simulation (Fig. 6). Just as expected, the single layer models had the lowest β-sheet contents. For the double and triple layer models, except 6, 8 and 9 chains, the other models had at least two residues among NFGAILS having sheet contents larger than 85%. Residues G24, A25 and I26 have a stronger tendency to form β-sheet. The results also indicate that the residues in the small size models have relatively lower β-sheet contents.

3.1.4. The stabilities of protofibril ends

The nematic order parameters, *P*2 [50], which describe the orientational order of the system and discriminate between ordered and disordered conformations, were considered here and the obtained results were shown in Fig. S5. In order to measure the detailed stabilities, we partition the protofibrils into three parts labeled as A, M, and B (end A, the middle part, end B), respectively (Fig. S5c). Fig. S5 shows that most of the *P*2 values of the two-layer models are larger than 0.6 indicating the formation of ordered conformations. However, end A or end B in some runs has low *P*2 values, which indicates that these ends are not very stable or they become disordered in some trajectories after 50 ns simulations. As for three-layer models, the *P*2 values for different

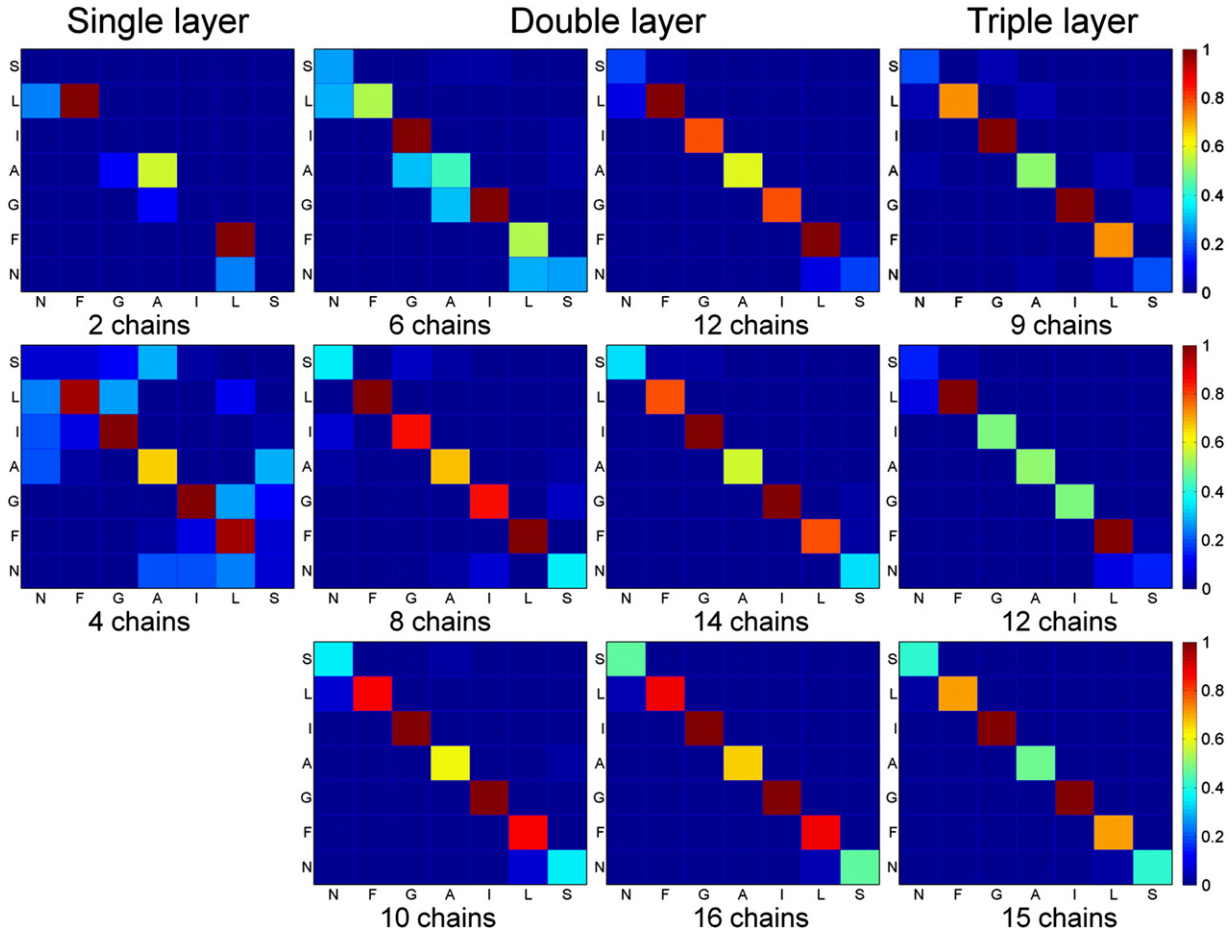

Fig. 3. H-bond contact map of $IAPP_{22-28}$ peptide in some representative trajectories. The number of main-chain hydrogen bonds is calculated during the last 25 ns and the largest one in each system is considered as 1 for reference.

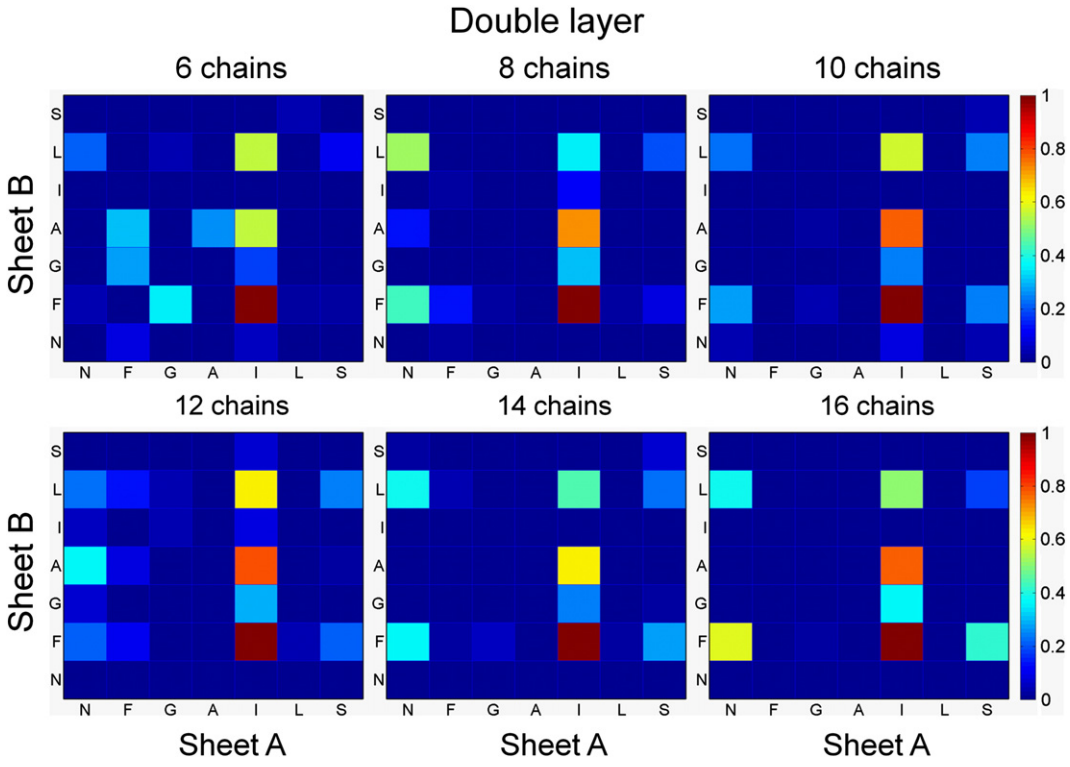

Fig. 4. Side chain contact map of double layer models in some representative trajectories during the last 25 ns. The horizontal axis represents sheet A, while vertical axis represents the other sheet, sheet B. The most contact between the two sheets in each system is considered as 1 for reference.

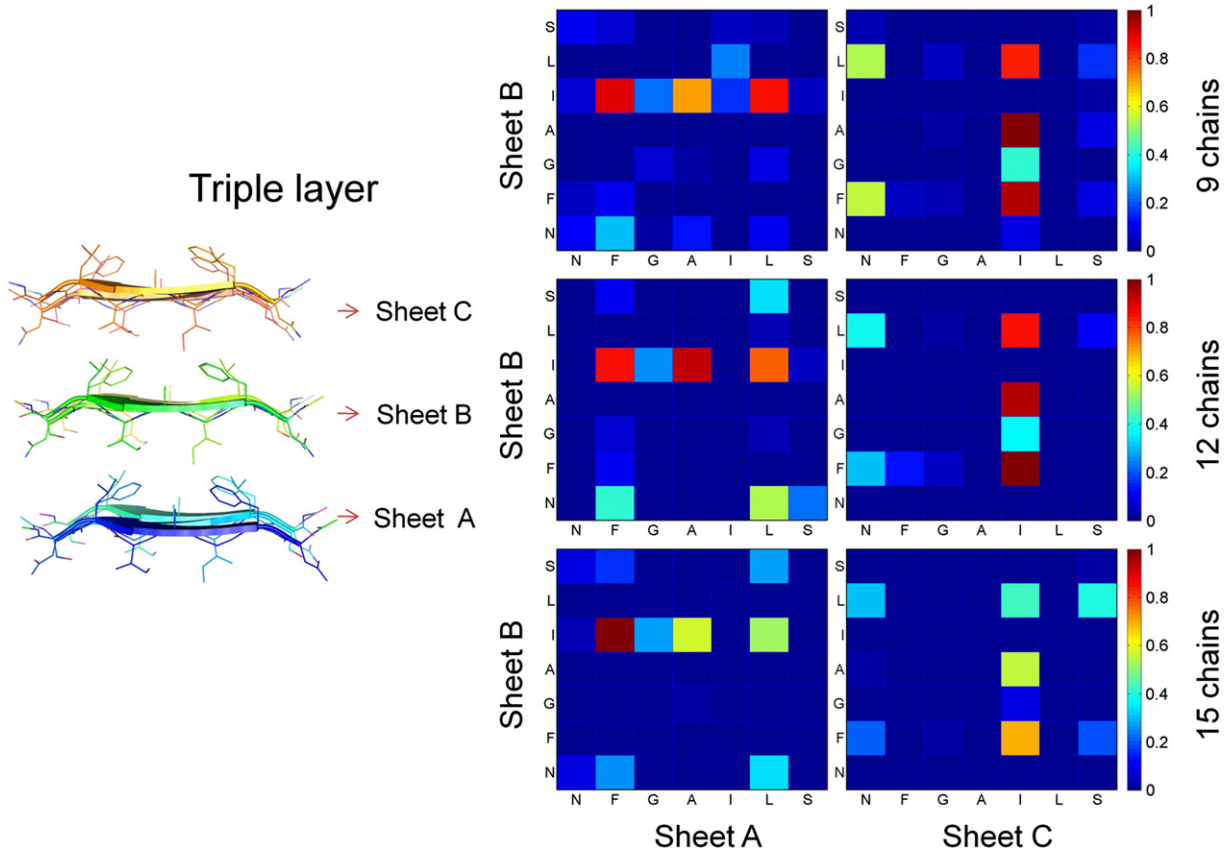

Fig. 5. Side chain contact map of triple layer models in some representative trajectories during the last 25 ns. The horizontal axis represents sheet A or sheet C, while vertical axis represents the middle sheet, sheet B. The most contact between two sheets in each system is considered as 1 for reference.

trajectories of the same model are different, which may be due to their instabilities and contribute to different mechanisms. As a whole, the two-layer models (8-mer to 16-mer) have more ordered conformations than the three-layer models (9-mer to 15-mer). The probability distribution of *P*2 values (Fig. 7) suggests that for two-layer models, one end and the middle part are more stable compared with the other end, while for the three-layer models, the distribution is disordered. This also indicates that the three-layer models are not very stable.

It is known that the formation of a nucleus is a reversible process dependent on the concentration of the peptide monomer. The oligomers might constantly form and dissolve [51]. In our present work, we only simulated the protofibrils with no extra free peptides around. In addition, the $IAPP_{22-28}$ fragment is very short, and the sheets are not aligned very well (Fig. 1). Hence, the edge peptides cannot be stabilized by the adjacent ones as the inner ones. Our results show that the overall oligomer stability increases with its size. However, in some systems, the edge peptides are not as stable as expected. When the sheet is composed of very few peptides, the inter-sheet interactions will not be very strong, and dislocations will occur along with simulation time causing the edge peptides more unstable, such as the hexamer (two-layer) and nonamer (three-layer). Furthermore, the stabilites of $IAPP_{22-28}$ oligomers are not only relevant to their size but also to their morphologies. For instance, all three-layer models are less stable compared with the corresponding two-layer models.

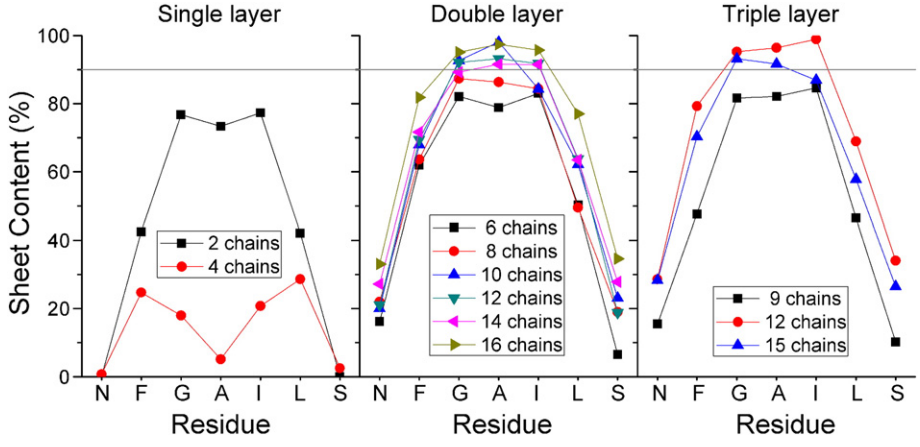

Fig. 6. Averaged β-sheet contents of each $IAPP_{22-28}$ residue during the last 10 ns.

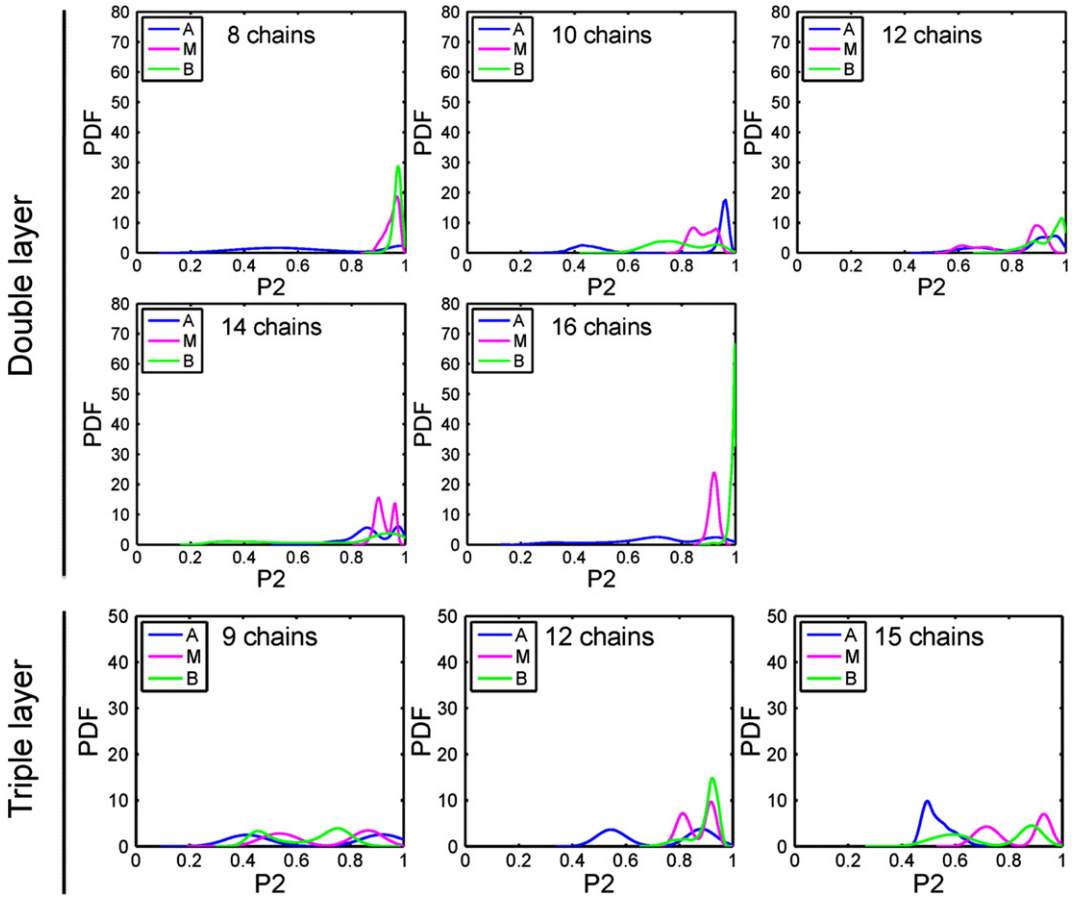

Fig. 7. Probability distribution of the *P*2 values averaged by all runs for each system. Only the last 5 ns simulations are considered.

3.2. The dynamics association of peptides from disordered state

As we know, the aggregation process is a slow process. Firstly, the change of a peptide chain from either a random or an ordered conformation to a β-conformation is a slow process. Secondly, the aggregation of peptides to a stable seed is a considerably slower process and takes a very long time to incubate to reach its formation. Therefore, it is very difficult to obtain a stable oligomer directly from all-atom simulations of random peptide conformations in our present study. Furthermore, the more the peptides involved in the aggregation simulation, the longer the time to obtain a stable oligomer is. So, here, for simulations of the aggregation process, only tetramer and octamer were considered. As Fig. 8 shows, the initial coil structures quickly convert into β-sheet structures, suggesting that $hIAPP_{22-28}$ has a strong propensity to form β-sheet. To explore the role of hydrogen bonds in the aggregation of $hIAPP_{22-28}$, the number of backbone hydrogen bonds between peptides was monitored and given in Fig. 9. It can be seen that the hydrogen-bond (H-bond) number for 4 peptides increases and achieves a balance after the first 25 ns, and for the 8 peptides it increases more quickly in the initial phase. At the beginning, all of the peptides are in disordered structure state, and the number of H-bonds is very small, while later, most of the peptides are converted into extended conformations

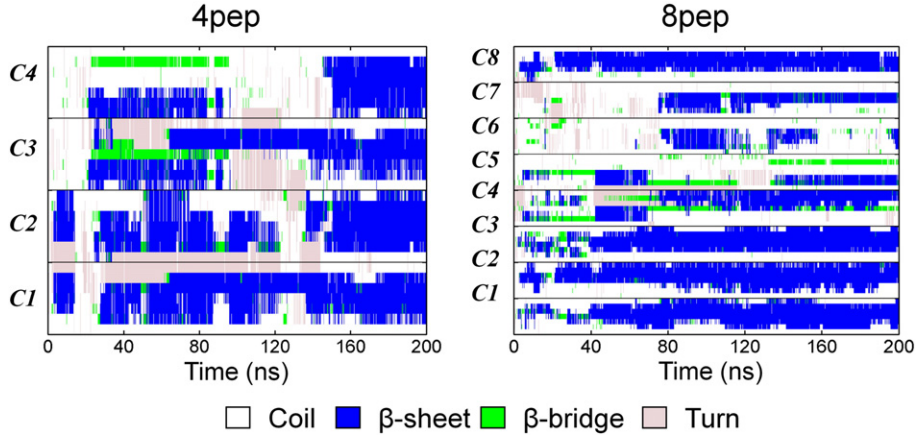

Fig. 8. Graphical representation of secondary structure analysis for 4 and 8 $IAPP_{22-28}$ peptides. The peptides are labeled as C1 to C4 and C1 to C8, respectively.

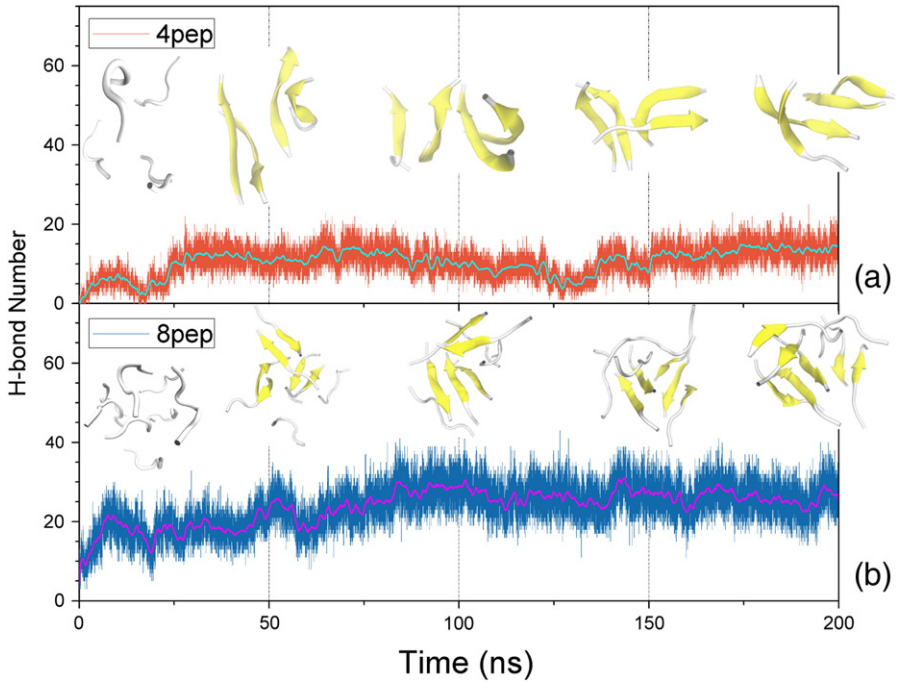

Fig. 9. a, b) The number of backbone hydrogen bonds was plotted as a function of simulation time and structural evolution (0 ns, 50 ns, 100 ns, 150 ns, 200 ns) was shown. The peptides were shown as cartoon: β-sheet in yellow, and others in white.

(Fig. 8). Our results suggest that H-bonds for 8-peptide model are more stable than those for 4 peptides. In addition, the H-bond number and β-sheet content have the same change tendency, which indicates that H-bond interaction plays an important role in the formation of $hIAPP_{22-28}$ β-sheet-rich oligomers.

In summary, $hIAPP_{22-28}$ peptides are inclined to form partially ordered β-sheet-rich oligomers with high β-sheet contents for both 4 and 8 peptides. Although the aggregation runs suggest that the tetramer and octamer have high β-sheet contents, they continually adjust their conformations during the aggregation simulations, consistent with previous studies [51,52].

By connecting the aggregation simulations and the simulations of stability test, for the stability of octamer with double layers, although octamer cannot maintain a very stable oligomer state, it still can keep the oligomerization state with high beta sheet content. In the aggregation simulation of 8 peptides, partially ordered two-layer β-sheet-rich octamers are observed. As for tetramer, as we observed, the single-layer tetramer is certainly unstable. It almost loses the original secondary structure and converted to coil structure after 50 ns simulation. To further test the stability of tetramer, we performed the tetramer with double-layer arrangement. As Fig. S6 shows, the tetramer with double-layer structure persists high beta-sheet content although the double sheet twists largely, which is consistent with our aggregation simulation of 4 peptides. Consistent with a previous research [53], our results also demonstrate that a two-layer β-sheet cannot be formed with only 4 small chains, but a β-sheet-rich tetramer can be formed (Fig. 9). So, overall, the aggregation simulations are in line with the simulations of stability test of the studied oligomers.

4. Discussion

In recent years, there have been considerable experimental efforts devoted to determine the detailed atomic structure of amyloid fibrils, as well as the mechanisms and the driving forces for peptide self-assembly. Because of experimental difficulties, computer simulations provide a much-needed complement to existing experimental studies and offer precise predictions that serve as a basis for further experimental studies.

Amyloid formation with a “nucleated growth” mechanism by which proteins assemble into highly ordered amyloid fibrils poses several intriguing questions. First, what is the conformation of the seed and its minimal size? Second, what is the mechanism by which the seed forms and amyloid grows? Third, what is the driving force of amyloid formation? An answer to one of these problems would aid in illuminating the others. In order to obtain a clear understanding of the amyloid-forming mechanism, simulations were performed on distinct polypeptides using different levels of chain representation and different molecular dynamics approaches [8,19–20,54–61]. For example, Wei' group [54] conducted coarse-grained MD simulations for the β2m83–89 NHVTLSQ and Aβ16–22 KLVFFAE fragments. Their results indicate that the critical nucleation size from which rapid fibril growth occurs is very likely larger than 8 chains for both peptides. However, Teplow and co-workers [62] reported that kinetic models of amyloid formation fit time-course data when the number of chains involved in the aggregation nucleus for Aβ aggregation is set to 10 chains. In agreement with that, it's reported that below this critical nucleus the edge chains of the 4-, 6-, and 8-chain protofibrils are instable, shifting the populations from ordered fibril C_n to populations with increased free monomer C_{n-1} [23].

Additionally, in recent years, much effort has been spend on the fibril formation of the NFGAIL peptide ($IAPP_{22-27}$), which is a good model system and forms amyloid fibrils similar to those formed by the full-length IAPP polypeptide. Wu and co-workers carried MD simulations to investigate the early-stage aggregation on $IAPP_{22-27}$ systems containing either four peptides or a single peptide [51], four dimer subunits [52], and to probe the β-sheet elongation process [63]. And they observed partially ordered tetramers and well-ordered octamers. As in the elongation study, they did not observe significant preference toward either parallel or antiparallel β-sheets at the elongation stage in the restrained simulations, while in the unrestrained simulations, the dominant growth mode was disordered aggregation. However, the work of Zanuy et al. [60] suggests that the most stable conformation is an antiparallel strand orientation within the sheets and parallel between

sheets, and established that an oligomer of 6–9 $IAPP_{22-27}$ peptides is stable enough to be a seed. Starting from a preformed parallel dimer and ten disordered chains, the $IAPP_{22-27}$ peptides form essentially amorphous oligomers or more rarely ordered β-sheet structures indicating that a dimer is not a sufficient seed for avoiding amorphous aggregates [24].

Our simulations for the stabilities of $IAPP_{22-28}$ oligomers show that the one-layer model and the three-layer models are not as stable as expected. Although the peptides remain associated, the native backbone H-bond and side-chain contact networks are weaken or broken at the end of the simulation. As for the two-layer models, some runs of them lost one edge chain, but the other part of them still maintained stable β-sheet rich conformation. Hence, we think with the same number of chains per sheet that the two-layer models are more stable than the three-layer ones. Generally speaking, the smaller β-sheet oligomers with no more than 10 peptides are less stable.

Many amino acid sequences can assemble into amyloid fibril, further lead to the occurrence of diseases. Thus, it is necessary to understand how this process happens and what are the driving forces promoting this process. It is well established that the propensity to form fibrils highly depends on the pH, ionic strength, and concentration of the solution. In addition, macromolecular crowding [64] can also influence the amyloid aggregation. In general, self-assembly is driven by noncovalent interactions, including Van der Waal's forces, hydrogen bonding, Coulombic interactions, and hydrophobic effects. Hydrophobic residues with high propensities to form β-strand conformation and residues with complementary charges promote fibril formation, and positively and negatively charged peptides can copolymerize. It appears that a delicate balance between hydrophobic forces [11,59], Coulombic interactions [65], and secondary structure propensities [17,65] is involved in the formation of fibrils.

The fibril-forming sequences KFFE and KVVE show partial β-strand conformation in solution, whereas the non-fibril-forming sequences KLLE and KAAE show random structure only, suggesting that inherent propensity for β-strand conformation promotes fibril formation [65]. The peptides KFFK or EFFE do not form fibrils on their own but do so in an equimolar mixture. Thus, intermolecular electrostatic interactions, either between charged dipolar peptides or between complementary charges of co-fibrillating peptides favor fibril formation [65]. There is also strong experimental evidence that aromatic interactions resulting from the phenylalanine and tyrosine rings play a crucial role in amyloid formation [66,67]. For instance, KFFE forms fibrils, but KLLE does not [65]. The work by Wu and co-workers [52] also suggests that F23 plays an essential role in the formation of ordered oligomers, so an aromatic inhibitor may prevent the amyloid seed formation by inhibiting β-sheet stacking, for example, phenol red [68], congo red [69] and esveratrol [70]. Our previous work [71] also showed that carbon nanoparticles can inhibit the aggregation of $IAPP_{22-28}$, and F23 played an important role in the adsorption process. However, based on the experimental method, the study [72] on the F15L/F23L/Y37L triple mutant of IAPP indicated that aromatic residues were not an absolute requirement for amyloid formation by IAPP, but they did influence the rate of fibril formation and fibril morphology. In our $hIAPP_{22-28}$ protofibril models, F23 does not contact with the other F23 residues. Therefore, in our study, the high hydrophobicity of F23 is more important.

Additionally, our mechanism also displays the crucial role of the main-chain H-bonds in guiding the peptides to fully ordered aggregates. For protofibrils, breaking native H-bond network will destabilize their structures. This result is consistent with the previous experimental study that high urea concentration will destabilize $Aβ_{16-22}$ (KLVFFAE) oligomers as well as other amyloidogenic peptides largely depending on hydrogen bond formation between urea and the peptide backbone [73].

Generally speaking, nonnative side-chain electrostatic and hydrophobic interactions bring the peptides together, which allow the native backbone–backbone H-bond interactions to start the assembly of β-sheets. Once these are formed, the final organization appears to be driven by native side chain–side chain interactions. Furthermore, the formation is sequence-specific.

5. Conclusions

Our simulations probing the stability and formation of the $IAPP_{22-28}$ oligomers are a simplification of complex amyloid formation. Nevertheless, it enables us to address several key questions: how is the initial seed stabilized and formed? What are the driving forces, hydrogen bonds, hydrophobicity or others? What is the smallest size of a nucleus? Through the simulations, we found that the driving forces to form and stabilize an oligomer are the hydrophobic effect and backbone H-bond interaction. Our results also indicate that the ordered protofibrils with no more than 16 $hIAPP_{22-28}$ chains will be structurally stable in two layers, while one-layer or three-layer models are not stable as expected. Based on the obtained results, we found that the stability of an $IAPP_{22-28}$ oligomer was not only related with its size but also with its arrangements. In many cases, as the edge chains are not binding tightly to the rest part as the inner peptides, during simulations, some of them are lost. Furthermore, the aggregation simulations show that the initial coil structures of peptides can quickly aggregate and convert to partially ordered β-sheet-rich oligomers. Our simulations also indicate that $IAPP_{22-28}$ peptides tend to form an antiparallel strand orientation within the sheets.

Acknowledgements

This work was supported by the National Natural Science Foundation of China (Grant no: 21103075) and the Natural Science Foundation of Gansu Province, China (Grant no: 1208RJYA034). We would like to thank the Gansu Computing Center for providing the computing resources.

Appendix A. Supplementary data

Supplementary data to this article can be found online at http://dx.doi.org/10.1016/j.bbagen.2013.09.012.

References

[1] F. Chiti, C. Dobson, Protein misfolding, functional amyloid, and human disease, Annu. Rev. Biochem. 75 (2006) 333–366.
[2] M. Stefani, Protein aggregation diseases: toxicity of soluble prefibrillar aggregates and their clinical significance, Methods Mol. Biol 648 (2010) 25–41.
[3] M. Stefani, C.M. Dobson, Protein aggregation and aggregate toxicity: new insights into protein folding, misfolding diseases and biological evolution, J. Mol. Med. 81 (2003) 678–699.
[4] C.G. Glabe, Common mechanisms of amyloid oligomer pathogenesis in degenerative disease, Neurobiol. Aging 27 (2006) 570–575.
[5] R. Kayed, E. Head, J.L. Thompson, T.M. McIntire, S.C. Milton, C.W. Cotman, C.G. Glabe, Common structure of soluble amyloid oligomers implies common mechanism of pathogenesis, Science 300 (2003) 486–489.
[6] M.R. Sawaya, S. Sambashivan, R. Nelson, M.I. Ivanova, S.A. Sievers, M.I. Apostol, M.J. Thompson, M. Balbirnie, J.J.W. Wiltzius, H.T. McFarlane, A.O. Madsen, C. Riekel, D. Eisenberg, Atomic structures of amyloid cross-beta spines reveal varied steric zippers, Nature 447 (2007) 453–457.
[7] A. Vitalis, A. Caflisch, Micelle-like architecture of the monomer ensemble of Alzheimer's amyloid-β peptide in aqueous solution and its implications for Aβ aggregation, J. Mol. Biol. 403 (2010) 148–165.
[8] A. Vitalis, N. Lyle, R.V. Pappu, Thermodynamics of beta-sheet formation in polyglutamine, Biophys. J. 97 (2009) 303–311.
[9] B. Strodel, C.S. Whittleston, D.J. Wales, Thermodynamics and kinetics of aggregation for the GNNQQNY peptide, J. Am. Chem. Soc. 129 (2007) 16005–16014.
[10] J. Gsponer, U. Haberthür, A. Caflisch, The role of side-chain interactions in the early steps of aggregation: molecular dynamics simulations of an amyloid-forming peptide from the yeast prion Sup35, Proc. Natl. Acad. Sci. 100 (2003) 5154–5159.
[11] W. Hwang, S. Zhang, R.D. Kamm, M. Karplus, Kinetic control of dimer structure formation in amyloid fibrillogenesis, Proc. Natl. Acad. Sci. 101 (2004) 12916–12921.
[12] M. López de la Paz, G.M.S. de Mori, L. Serrano, G. Colombo, Sequence dependence of amyloid fibril formation: insights from molecular dynamics simulations, J. Mol. Biol. 349 (2005) 583–596.
[13] M. Cecchini, R. Curcio, M. Pappalardo, R. Melki, A. Caflisch, A molecular dynamics approach to the structural characterization of amyloid aggregation, J. Mol. Biol. 357 (2006) 1306–1321.

[14] A. De Simone, L. Esposito, C. Pedone, L. Vitagliano, Insights into stability and toxicity of amyloid-like oligomers by replica exchange molecular dynamics analyses, Biophys. J. 95 (2008) 1965–1973.
[15] R. Pellarin, A. Caflisch, Interpreting the aggregation kinetics of amyloid peptides, J. Mol. Biol. 360 (2006) 882–892.
[16] G. Bellesia, J.-E. Shea, Self-assembly of beta-sheet forming peptides into chiral fibrillar aggregates, J. Chem. Phys. 126 (2007) 245104–245111.
[17] G. Bellesia, J.-E. Shea, Effect of β-sheet propensity on peptide aggregation, J. Chem. Phys. 130 (2009) 145103–145110.
[18] K.L. Osborne, M. Bachmann, B. Strodel, Thermodynamic analysis of structural transitions during GNNQQNY aggregation, Proteins Struct. Funct. Bioinform. (2013), http://dx.doi.org/10.1002/prot.24263.
[19] B. Ma, R. Nussinov, Stabilities and conformations of Alzheimer's β-amyloid peptide oligomers (Aβ16–22, Aβ16–35, and Aβ10–35): sequence effects, Proc. Natl. Acad. Sci. 99 (2002) 14126–14131.
[20] N.-V. Buchete, R. Tycko, G. Hummer, Molecular dynamics simulations of Alzheimer's β-amyloid protofilaments, J. Mol. Biol. 353 (2005) 804–821.
[21] C. Wu, M.T. Bowers, J.-E. Shea, Molecular structures of quiescently grown and brain-derived polymorphic fibrils of the Alzheimer amyloid Aβ 9–40 peptide: a comparison to agitated fibrils, PLoS Comput. Biol. 6 (2010) e1000693.
[22] R. Pellarin, E. Guarnera, A. Caflisch, Pathways and intermediates of amyloid fibril formation, J. Mol. Biol. 374 (2007) 917–924.
[23] N.L. Fawzi, Y. Okabe, E.H. Yap, T. Head-Gordon, Determining the critical nucleus and mechanism of fibril elongation of the Alzheimer's Aβ1–40 peptide, J. Mol. Biol. 365 (2007) 535–550.
[24] A. Melquiond, J.-C. Gelly, N. Mousseau, P. Derreumaux, Probing amyloid fibril formation of the NFGAIL peptide by computer simulations, J. Chem. Phys. 126 (2007) 065101–065107.
[25] D. Matthes, B.L. De Groot, Secondary structure propensities in peptide folding simulations: a systematic comparison of molecular mechanics interaction schemes, Biophys. J. 97 (2009) 599–608.
[26] E. Cino, W.Y. Choy, M. Karttunen, Comparison of secondary structure formation using 10 different force fields in microsecond molecular dynamics simulations, J. Chem. Theory Comput. 8 (2012) 2725–2740.
[27] P.L. Freddolino, S. Park, B. Roux, K. Schulten, Force field bias in protein folding simulations, Biophys. J. 96 (2009) 3772–3780.
[28] R.B. Best, J. Mittal, Free-energy landscape of the GB1 hairpin in all-atom explicit solvent simulations with different force fields: similarities and differences, Proteins Struct. Funct. Bioinform. 79 (2011) 1318–1328.
[29] J. Mittal, R.B. Best, Tackling force-field bias in protein folding simulations: folding of villin HP35 and pin WW domains in explicit water, Biophys. J. 99 (2010) L26–L28.
[30] K.K. Patapati, N.M. Glykos, Three force fields' views of the 3_{10} helix, Biophys. J. 101 (2011) 1766–1771.
[31] P. Kührová, A. De Simone, M. Otyepka, R.B. Best, Force-field dependence of chignolin folding and misfolding: comparison with experiment and redesign, Biophys. J. 102 (2012) 1897–1906.
[32] R.B. Best, N.-V. Buchete, G. Hummer, Are current molecular dynamics force fields too helical? Biophys. J. 95 (2008) L07–L09.
[33] L. Wei, P. Jiang, W. Xu, H. Li, H. Zhang, L. Yan, M.B. Chan-Park, X.W. Liu, K. Tang, Y. Mu, The molecular basis of distinct aggregation pathways of islet amyloid polypeptide, J. Biol. Chem. 286 (2011) 6291–6300.
[34] E.T.A.S. Jaikaran, A. Clark, Islet amyloid and type 2 diabetes: from molecular misfolding to islet pathophysiology, BBA Mol. Basis Dis. 1537 (2001) 179–203.
[35] R.P.R. Nanga, J.R. Brender, S. Vivekanandan, A. Ramamoorthy, Structure and membrane orientation of IAPP in its natively amidated form at physiological pH in a membrane environment, BBA Biomembr. 1808 (2011) 2337–2342.
[36] D.F. Moriarty, D.P. Raleigh, Effects of sequential proline substitutions on amyloid formation by human amylin20–29, Biochemistry 38 (1999) 1811–1818.
[37] J. Madine, E. Jack, P.G. Stockley, S.E. Radford, L.C. Serpell, D.A. Middleton, Structural insights into the polymorphism of amyloid-like fibrils formed by region 20–29 of amylin revealed by solid-state NMR and X-ray fiber diffraction, J. Am. Chem. Soc. 130 (2008) 14990–15001.
[38] J.T. Nielsen, M. Bjerring, M.D. Jeppesen, R.O. Pedersen, J.M. Pedersen, K.L. Hein, T. Vosegaard, T. Skrydstrup, D.E. Otzen, N.C. Nielsen, Unique identification of supramolecular structures in amyloid fibrils by solid-state NMR spectroscopy, Angew. Chem. 121 (2009) 2152–2155.
[39] Z. Yang, B. Shi, H. Lu, P. Xiu, R. Zhou, Dewetting transitions in the self-assembly of two amyloidogenic β-sheets and the importance of matching surfaces, J. Phys. Chem. B 115 (2011) 11137–11144.
[40] D. Case, T. Darden, T. Cheatham III, C. Simmerling, J. Wang, R. Duke, R. Luo, M. Crowley, R. Walker, W. Zhang, AMBER 10, University of California, San Francisco, 2008.
[41] Y. Duan, C. Wu, S. Chowdhury, M. Lee, G. Xiong, W. Zhang, R. Yang, P. Cieplak, R. Luo, T. Lee, A point-charge force field for molecular mechanics simulations of proteins based on condensed-phase quantum mechanical calculations, J. Comput. Chem. 24 (2003) 1999–2012.
[42] M. Lee, Y. Duan, Distinguish protein decoys by using a scoring function based on a new AMBER force field, short molecular dynamics simulations, and the generalized born solvent model, Proteins Struct. Funct. Bioinform. 55 (2004) 620–634.
[43] W. Jorgensen, J. Chandrasekhar, J. Madura, R. Impey, M. Klein, Comparison of simple potential functions for simulating liquid water, J. Chem. Phys. 79 (1983) 926–935.
[44] U. Essmann, L. Perera, M.L. Berkowitz, T. Darden, H. Lee, L.G. Pedersen, A smooth particle mesh Ewald method, J. Chem. Phys. 103 (1995) 8577–8593.
[45] J.P. Ryckaert, G. Ciccotti, H.J.C. Berendsen, Numerical integration of the Cartesian equations of motion of a system with constraints: molecular dynamics of n-alkanes, J. Comput. Phys. 23 (1977) 327–341.
[46] H.J.C. Berendsen, J.P.M. Postma, W.F. Van Gunsteren, A. DiNola, J.R. Haak, Molecular dynamics with coupling to an external bath, J. Chem. Phys. 81 (1984) 3684–3690.
[47] W. Humphrey, A. Dalke, K. Schulten, VMD: visual molecular dynamics, J. Mol. Graph. 14 (1996) 33–38.
[48] D. Frishman, P. Argos, Knowledge-based protein secondary structure assignment, Proteins Struct. Funct. Bioinform. 23 (2004) 566–579.
[49] H. Li, Y. Luo, P. Derreumaux, G. Wei, Carbon nanotube inhibits the formation of β-sheet-rich oligomers of the Alzheimer's amyloid-β(16–22) peptide, Biophys. J. 101 (2011) 2267–2276.
[50] M. Cecchini, F. Rao, M. Seeber, A. Caflisch, Replica exchange molecular dynamics simulations of amyloid peptide aggregation, J. Chem. Phys. 121 (2004) 10748–10756.
[51] C. Wu, H. Lei, Y. Duan, Formation of partially ordered oligomers of amyloidogenic hexapeptide (NFGAIL) in aqueous solution observed in molecular dynamics simulations, Biophys. J. 87 (2004) 3000–3009.
[52] C. Wu, H. Lei, Y. Duan, The role of Phe in the formation of well-ordered oligomers of amyloidogenic hexapeptide (NFGAIL) observed in molecular dynamics simulations with explicit solvent, Biophys. J. 88 (2005) 2897–2906.
[53] A. Melquiond, G. Boucher, N. Mousseau, P. Derreumaux, Following the aggregation of amyloid-forming peptides by computer simulations, J. Chem. Phys. 122 (2005) 174904–174908.
[54] Y. Lu, P. Derreumaux, Z. Guo, N. Mousseau, G. Wei, Thermodynamics and dynamics of amyloid peptide oligomerization are sequence dependent, Proteins Struct. Funct. Bioinform. 75 (2009) 954–963.
[55] J. Zhang, M. Muthukumar, Simulations of nucleation and elongation of amyloid fibrils, J. Chem. Phys. 130 (2009) 035102–035117.
[56] G. Colombo, I. Daidone, E. Gazit, A. Amadei, A. Di Nola, Molecular dynamics simulation of the aggregation of the core-recognition motif of the islet amyloid polypeptide in explicit water, Proteins Struct. Funct. Bioinform. 59 (2005) 519–527.
[57] L. Cruz, B. Urbanc, J.M. Borreguero, N.D. Lazo, D.B. Teplow, H.E. Stanley, Solvent and mutation effects on the nucleation of amyloid β-protein folding, Proc. Natl. Acad. Sci. 102 (2005) 18258–18263.
[58] R. Vijayan, P.C. Biggin, Conformational preferences of a 14-residue fibrillogenic peptide from acetylcholinesterase, Biochemistry 49 (2010) 3678–3684.
[59] R.D. Hills Jr., C.L. Brooks Iii, Hydrophobic cooperativity as a mechanism for amyloid nucleation, J. Mol. Biol. 368 (2007) 894–901.
[60] D. Zanuy, B. Ma, R. Nussinov, Short peptide amyloid organization: stabilities and conformations of the islet amyloid peptide NFGAIL, Biophys. J. 84 (2003) 1884–1894.
[61] J. Nasica-Labouze, N. Mousseau, Kinetics of amyloid aggregation: a study of the GNNQQNY prion sequence, PLoS Comput. Biol. 8 (2012) e1002782.
[62] A. Lomakin, D.B. Teplow, D.A. Kirschner, G.B. Benedek, Kinetic theory of fibrillogenesis of amyloid β-protein, Proc. Natl. Acad. Sci. 94 (1997) 7942–7947.
[63] C. Wu, H. Lei, Y. Duan, Elongation of ordered peptide aggregate of an amyloidogenic hexapeptide NFGAIL observed in molecular dynamics simulations with explicit solvent, J. Am. Chem. Soc. 127 (2005) 13530–13537.
[64] A. Magno, A. Caflisch, R. Pellarin, Crowding effects on amyloid aggregation kinetics, J. Phys. Chem. Lett. 1 (2010) 3027–3032.
[65] L. Tjernberg, W. Hosia, N. Bark, J. Thyberg, J. Johansson, Charge attraction and β propensity are necessary for amyloid fibril formation from tetrapeptides, J. Biol. Chem. 277 (2002) 43243–43246.
[66] E. Gazit, A possible role for π-stacking in the self-assembly of amyloid fibrils, FASEB J. 16 (2002) 77–83.
[67] S.M. Tracz, A. Abedini, M. Driscoll, D.P. Raleigh, Role of aromatic interactions in amyloid formation by peptides derived from human amylin, Biochemistry 43 (2004) 15901–15908.
[68] C. Wu, H. Lei, Z. Wang, W. Zhang, Y. Duan, Phenol red interacts with the protofibril-like oligomers of an amyloidogenic hexapeptide NFGAIL through both hydrophobic and aromatic contacts, Biophys. J. 91 (2006) 3664–3672.
[69] C. Wu, Z. Wang, H. Lei, W. Zhang, Y. Duan, Dual binding modes of congo red to amyloid protofibril surface observed in molecular dynamics simulations, J. Am. Chem. Soc. 129 (2007) 1225–1232.
[70] P. Jiang, W. Li, J.-E. Shea, Y. Mu, Resveratrol inhibits the formation of multiple-layered β-sheet oligomers of the human islet amyloid polypeptide segment 22–27, Biophys. J. 100 (2011) 1550–1558.
[71] J. Guo, J. Li, Y. Zhang, X. Jin, H. Liu, X. Yao, Exploring the influence of carbon nanoparticles on the formation of β-sheet-rich oligomers of $IAPP_{22-28}$ peptide by molecular dynamics simulation, PLoS One 8 (2013) e65579.
[72] P. Marek, A. Abedini, B. Song, M. Kanungo, M.E. Johnson, R. Gupta, W. Zaman, S.S. Wong, D.P. Raleigh, Aromatic interactions are not required for amyloid fibril formation by islet amyloid polypeptide but do influence the rate of fibril formation and fibril morphology, Biochemistry 46 (2007) 3255–3261.
[73] D. Klimov, J.E. Straub, D. Thirumalai, Aqueous urea solution destabilizes Aβ16–22 oligomers, Proc. Natl. Acad. Sci. 101 (2004) 14760–14765.